

REPORT DOCUMENTATION PAGE

AFRL-SR-AR-TR-06-0051

Public reporting burden for this collection of information is estimated to average 1 hour per response, including the time for reviewing instructions, gathering existing data needed, and completing and reviewing this collection of information. Send comments regarding this burden estimate or any other aspect of this collection of information, including suggestions for reducing the burden, to Washington Headquarters Services, Directorate for Information Operations and Reports (0704-0188), 1215 Jefferson Davis Highway, Suite 1204, Arlington, VA 22202-4302, and to the Office of Management and Budget, Paperwork Project Director (0704-0188), 1215 Jefferson Davis Highway, Suite 1204, Arlington, VA 22202-4302. Respondents should be aware that notwithstanding any other provision of law, no person shall be subject to any penalty for failing to comply with a collection of information if it does not display this OMB control number. **PLEASE DO NOT RETURN YOUR FORM TO THE ABOVE ADDRESS.**

1. REPORT DATE (DD-MM-YYYY) 03/01/06		2. REPORT TYPE Final report		3. DATES COVERED (From - To) 12/01/01 - 05/31/05	
4. TITLE AND SUBTITLE COMPOSITES REINFORCED WITH SHORT WAVY FIBERS				5a. CONTRACT NUMBER	
				5b. GRANT NUMBER F49620-02-1-0018	
				5c. PROGRAM ELEMENT NUMBER	
6. AUTHOR(S) C. T. Sun, J. Cho, and A. Deo				5d. PROJECT NUMBER	
				5e. TASK NUMBER	
				5f. WORK UNIT NUMBER	
7. PERFORMING ORGANIZATION NAME(S) AND ADDRESS(ES) Purdue University West Lafayette, Indiana 47907				8. PERFORMING ORGANIZATION REPORT NUMBER	
9. SPONSORING / MONITORING AGENCY NAME(S) AND ADDRESS(ES) Air Force Office of Scientific Research 875 N. Randolph Street, Suite 325, Room Arlington, VA 22203 <i>Dr. Byunghip Lee NA</i>				10. SPONSOR/MONITOR'S ACRONYM(S)	
				11. SPONSOR/MONITOR'S REPORT NUMBER(S)	
12. DISTRIBUTION / AVAILABILITY STATEMENT DISTRIBUTION UNLIMITED DISTRIBUTION STATEMENT A Approved for Public Release Distribution Unlimited					
13. SUPPLEMENTARY NOTES					
14. ABSTRACT In short fiber composites including nanocomposites, the load transfer efficiency among fibers is crucial in effecting superior composite properties. It is conceivable that this load transfer efficiency depends on the shape, aspect ratio, and surface area of the fiber. The effect of surface area of the reinforcing element is of particular importance because of the increasing use of nano particles in nanocomposites. It is well known that for the same volume, a material at nano scale possesses much greater surface areas than at larger scales. It is evident that more surface areas mean more load transfer paths and, thus, lower interfacial stresses between the reinforcement and the matrix. The lowering of interfacial stresses is expected to lead to higher composite strengths. In this research project we used model composites to reach the following conclusions: 1) Wavy fibers lower the interfacial stresses and thus increase the composite strength significantly; 2) for the same fiber volume fraction, the composite with thinner fibers has higher strength than the composite with thicker fibers, 3) result of fiber (platelet) pull-out tests indicates that thinner fibers gave a higher pull out strength than thicker fibers. The increase was about 30% for each 50% reduction in the thickness of the fiber, 4) the Young's modulus of a particulate composite is not influenced by the size of the particle if it is of micron or larger sizes. However, the composite Young's modulus is enhanced with decreasing particle sizes at nano scale. This behavior was explained by using molecular dynamics simulations which revealed that this enhancement of modulus by nanoparticles may be attributed to a stiffer polymer layer formed around nanoparticles.					
15. SUBJECT TERMS					
16. SECURITY CLASSIFICATION OF:			17. LIMITATION OF ABSTRACT	18. NUMBER OF PAGES	19a. NAME OF RESPONSIBLE PERSON
a. REPORT UNCLASSIFIED	b. ABSTRACT UNCLASSIFIED	c. THIS PAGE UNCLASSIFIED		30	C. T. Sun
					19b. TELEPHONE NUMBER (include area code) 765-494-5130

Final Report

COMPOSITES REINFORCED WITH SHORT WAVY FIBERS

AFOSR GRANT # F49620-02-1-0018

Prepared by

C.T. Sun, J. Cho, and A. Deo
School of Aeronautics and Astronautics
Purdue University
West Lafayette, IN 47907

Submitted to
AFOSR

Mechanics of Materials & Devices
4015 Wilson Boulevard, AFOSR/NA, Room 713
Arlington, VA 22203-1954

20060309 074

March 1, 2006

DISTRIBUTION STATEMENT A
Approved for Public Release
Distribution Unlimited

Part I: EFFECT OF FIBER SHAPE

I.1 Introduction

In short fiber composites, the load transfer efficiency among fibers is crucial in effecting superior composite properties. It is conceivable that this load transfer efficiency depends on the shape, aspect ratio, and surface area of the fiber. Recently, some researchers have used short fibers with two enlarged ends to reinforce polymer composites [I.1-I.2], and demonstrated the potential to improve significantly both strength and fracture toughness of the composite. The primary toughening mechanism provided by the bone-shaped short fiber is the large scale deformation in the surrounding matrix as the enlarged fiber ends pull out. In an earlier study, Zeng and Sun [I.3] found that a wavy lap joint configuration could yield much greater joint strengths than the conventional flat lap joints. This improvement in strength of the wavy joint was found to be the result of the interfacial stresses that were altered by the wavy geometry. The aforementioned success in wavy lap joints has motivated the present study in the shape of the reinforcement. The effect of surface area of the reinforcing element is of particular importance because of the increasing use of nano particles to form nanocomposites. It is well known that for the same volume, a material at nano scale possesses much greater surface areas than at larger scales. It is evident that more surface areas mean more load transfer paths and, thus, lower interfacial stresses between the reinforcement and the matrix. The lowering of interfacial stresses is expected to lead to higher composite strengths.

The objective of this research is to study the efficiency of load transfer in short fibers in composite materials. The variables of the reinforcement such as its shape and surface area/weight ratio are investigated both theoretically and verified experimentally. It is anticipated that the result of this research will benefit the design of the conventional short fiber composites as well as the emerging nanocomposites in which nano particles have extremely high surface/volume ratios.

Platelet type reinforcements are considered. Attention is focused on the effect of shape and surface area of the platelet on the mechanical properties of the composite. To simplify the experiment and observation, model composites are manufactured with platelets whose lateral dimensions are on the order of centimeters and thickness in the range of 0.01 - 1.0 mm. Micromechanics models are developed to help us understand the load transfer mechanisms and to achieve the optimal platelet shape and thickness.

I.2 Experiments

For ease of processing and fabrication, we chose a metal fiber based composite system. The straight and the wavy fibers were made using the Aluminum 6061 alloy. An aluminum sheet of 0.8mm (0.032 inch) in thickness was cut into 4.6mm wide strips using a water jet. The surface preparation of the aluminum strips involved drying at 220° F for about an hour so as to remove the moisture. The surface of the strip was then sanded by a sand paper hence removing the oxide layer covering the surface and was then thoroughly cleaned by acetone. The strip was then cut into short platelets of 20mm in length by using a shear cutter. For the preparation of wavy fibers, the straight aluminum strip was

compressed using a rigid mould yielding a bent shape as shown in Figure I.1. The bent strips were then cleaned again. Each wavy fiber (platelet) has a wavy part of 3mm at each end and inclined at 15° to the center portion. The dimensions of the straight as well as wavy fibers are given in Figure I.1.

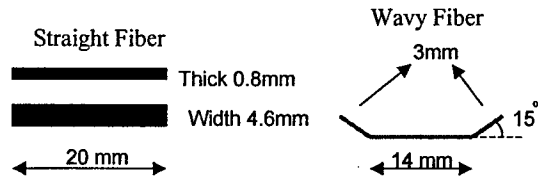


Figure I.1: Geometries of the straight fiber and wavy fiber

In the next step the short straight fibers (platelets) were glued in a sequence to form a long chain with the same epoxy to be used as the matrix for the composite. Fibers were aligned one over another as shown in Figure I.2 (for the chain of straight and wavy fibers). The epoxy is made by fully mixing Thermoset resin No. 66 and hardener with a mixing ratio by weight of 1:1. The chain of wavy fibers was constructed in a similar manner. Note that the overlap length was maintained at 3 mm for both types of fibers. The epoxy was allowed to cure at room temperature for 24 hrs. After proper curing of the epoxy, the chains were arranged in a mould using a spacer at each end to hold the fiber chains in place so as to ensure a uniform spacing between the chains. Figure I.3 shows straight fiber chains in the mould before mixing with epoxy. The amount of the epoxy cast into the mould was controlled to maintain the same thickness (7 mm) of the specimen and, thus, the same fiber volume fraction of the specimens. The epoxy was cured at room temperature for 24 hrs and post cured at 150°F for 3 hrs. The final composite specimen contained three chains of fibers with a fiber volume fraction of 6%.

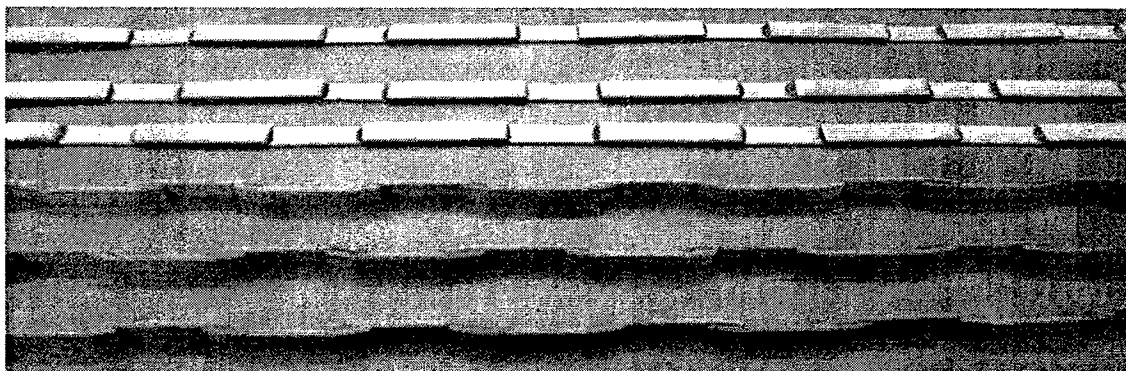


Figure I.2 Chain of straight fibers and wavy fibers

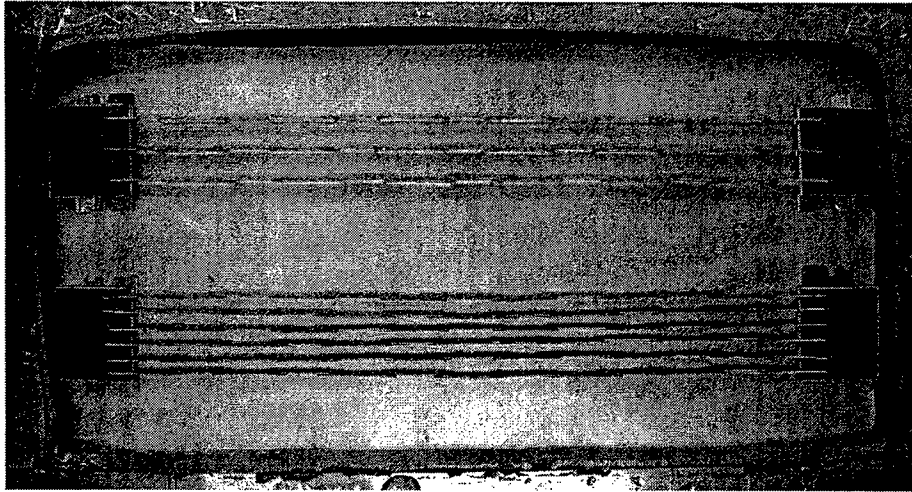


Figure I.3 Straight fiber chains in the mould

Once fully cured, the specimen was cut to the desired width (35 mm) and length (200 mm). Tensile properties were measured using an MTS testing machine. A constant displacement of 0.005mm/s was employed for all the samples. All of the specimens experienced a sudden failure. The stress-strain curves up to failure of straight and wavy fiber composites are shown in Figure I.4.

Failure strengths of each type of composite are compared in Table I.1. It is seen that the average strength of the wavy-fiber composite is greater than the straight-fiber composite by 73%.

Table I.2 compares the Young's moduli of the tensile specimens. Young's modulus was determined from the slope of the stress-strain curve in the strain range of 0.02%-0.1%. This was chosen as the materials exhibited linear stress-strain behavior within this range. On average the Young's modulus of the straight fiber specimen is about 8 % higher than the straight-fiber specimen.

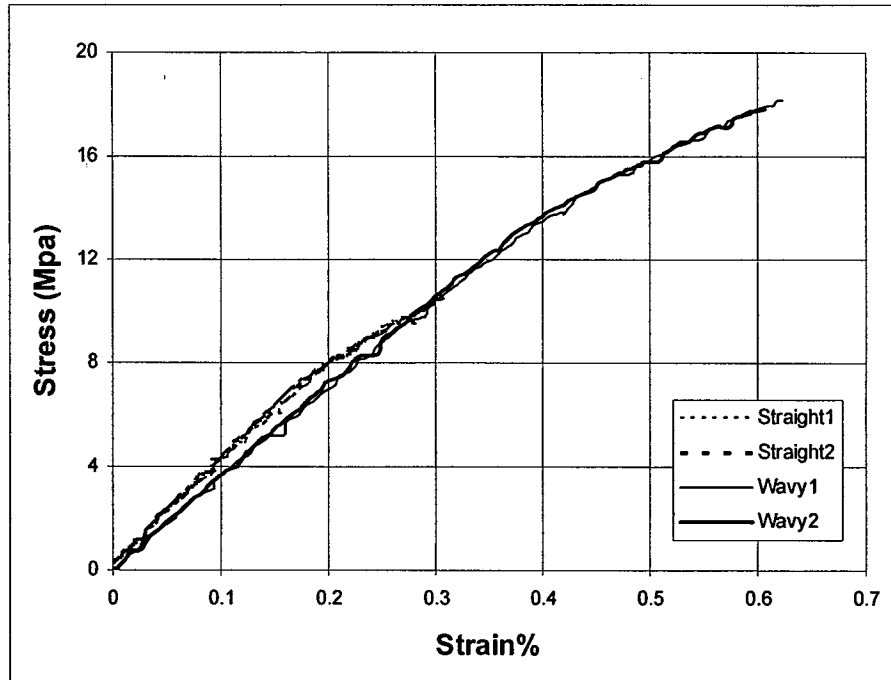


Figure I.4 Stress-strain curves for composites with straight fibers and with wavy fibers

Table 1: Failure strengths of straight and wavy fiber short fiber composites

Sample #	Straight Fiber (MPa)	Wavy Fiber (MPa)
1	10.23	18.16
2	10.53	17.80
Average	10.38	17.98

Table 2: Young's moduli of straight and wavy fiber short fiber composites

Sample #	Straight Fiber (GPa)	Wavy Fiber (GPa)
1	4.13	3.78
2	4.10	3.86
Average	4.12	3.84

I.3 Analysis of Interfacial Stresses

To understand why the wavy fiber composite outperformed the straight fiber composite in strength, finite element analyses were performed on a unit cell for each type of composite. Proper boundary conditions must be applied in order to ensure the periodicity condition so that the result of based on the unit cell can represent the global property of the composite. The Linear Plane Strain Elements (Q4-4noded linear quadrilateral) in the commercial FE code ABAQUS were used for the analysis. The area inside the overlap was finely meshed so as to correctly capture the stress-strain distributions. Of interest are interfacial stresses along the overlap of the adjacent fibers. Figures I.5 and I.6 show the

distributions of the interfacial normal and shear stresses in the overlap region between two fibers, respectively. Note that these stress components are referenced to the local tangential and normal directions of the fiber. From Figure I.5 we note that the interfacial normal stress in both type of specimens are tensile and exhibit significant stress concentrations at the edge of the overlap. The stress concentration in the wavy fiber composite is seen to be less severe as compared with that in the straight fiber composite. In Figure I.6 we see that the level of interfacial shear stresses in the straight fiber composites is about 80% higher than the interfacial stresses in the wavy fiber composite. From the result of the FEA, it is evident that interfacial stresses between the wavy fibers are much smaller than those between the straight fibers. This characteristic explains why the composite with wavy fibers are stronger than the composite with straight fibers.

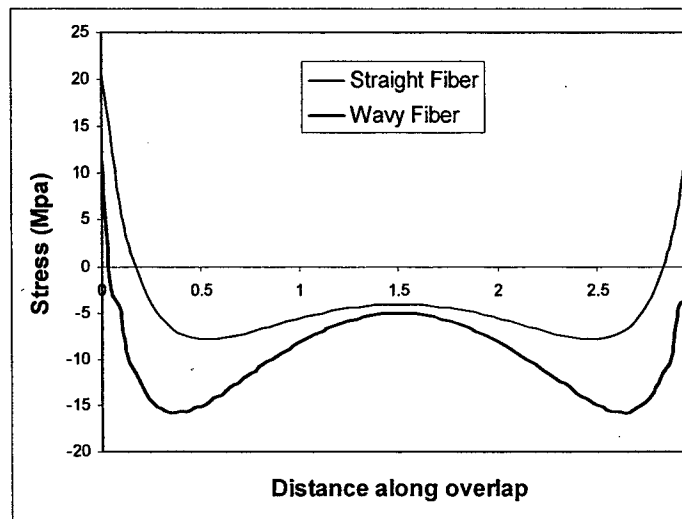


Figure I.5 Interfacial normal stress distributions in the fiber overlap region

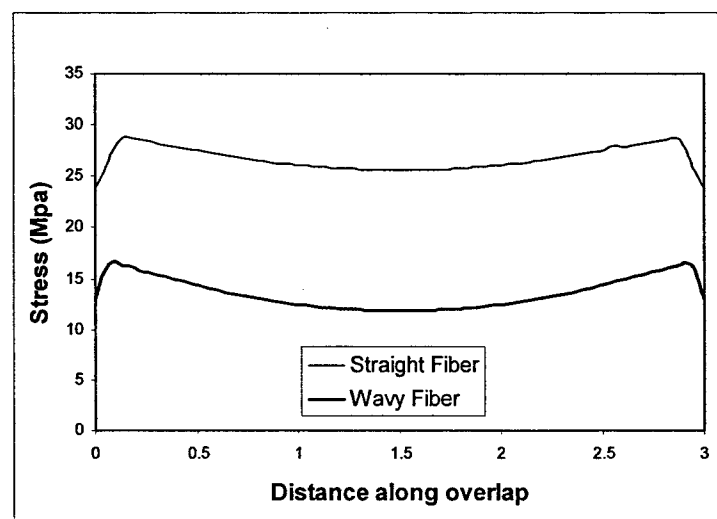


Figure I.6 Interfacial shear stress distributions in the fiber overlap region

I.4 Effect of Fiber Surface/Volume Ratio

In the composite, load in the matrix is to be transferred to the fiber. This load transfer has to take effect through the fiber/matrix interface. Thus, it is reasonable to expect good results if the fiber has a large surface area for a given volume. This is one of the reasons why nano materials are attractive as reinforcements for composites.

The objective of this part of the research is to experimentally verify this concept using a model composite and to develop a micromechanics model to explain this effect. The model composite selected is basically the same as the straight fiber composite discussed in Section II except for a few variations. First, copper was used make fiber chips in the experiment because of its availability in thin gages. Copper panels of 0.25 mm (0.01 inch) and 0.5 mm (0.02 inch) in thickness were cut by a water-jet into 4.7 mm-wide strips. Subsequently, the strips were cut into 2 cm chips. These chips were bonded into a chain using the epoxy that was later used as the matrix of the composite. The overlap length was 3 mm. For the composite specimen with thicker copper chips, there were three chains of fibers with 10 mm spacing between adjacent fibers as shown in Figure I.7. For the thinner fiber composite specimen, there were six fiber chains with 5 mm fiber spacing. The specimen width was 30 mm and thickness was 7 mm. The fiber volume fraction was 4% for both types of composites.

Tension tests were conducted on these two types of specimens with a displacement loading rate of 0.003 mm/s. Initially coupon specimens with straight edges were used and failure always occurred near the grips. Later, dog bone shaped specimens as shown in Figure I.7 were used in the test. The stress-strain curves up to failure are shown in Figure I.8. The strength data are listed in Table I.3.

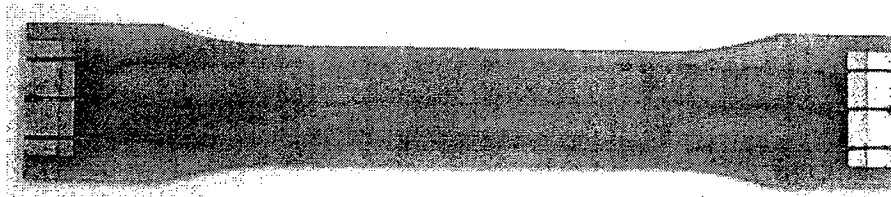


Figure I.7 Composite specimen made of 0.5 mm thick copper fiber chains

Table I.3 Failure strengths of thin and thick short fiber composites

Sample #	Thin Fiber (MPa)	Thick Fiber (MPa)
1	43.32	24.72
2	43.33	23.48
Average	43.33	24.10

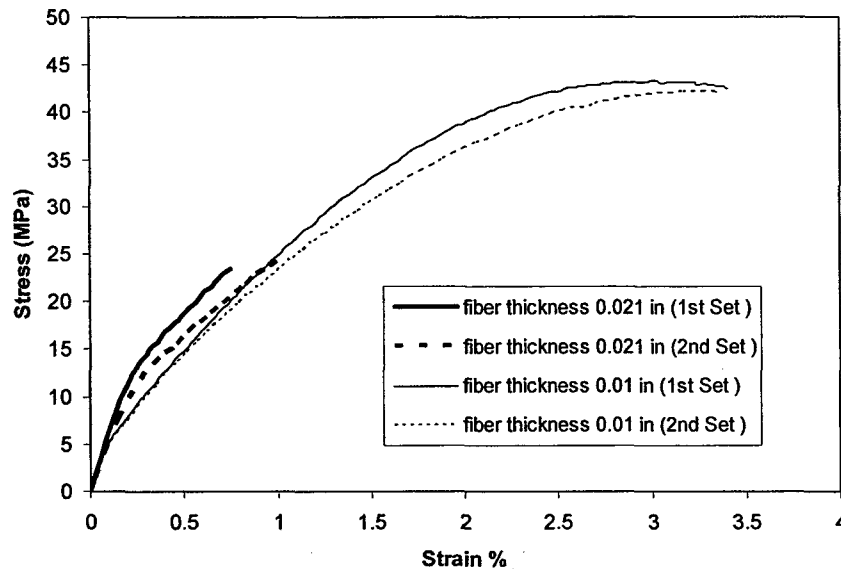


Figure I.7 Tensile test result for composites with thin and thick fibers

The experimental result clearly indicates that, for the same volume fraction of fibers, thin platelet fibers yield significantly higher composite strengths than thick fibers. The stress-strain curves in Figure I.7 also indicate that the specimens with thick fibers seem to have a higher stiffness than the ones with thin fibers. This is because the specimens with thin fibers have better load transfer than the ones with thick fibers. The thin copper fibers carried more load and reached yielding stress much earlier than the thick fiber. As a result in the specimens, the specimens with thick fibers seem to have a higher stiffness than the ones with thin fibers.

I.5 Conclusion

The following conclusions have been obtained from the results obtained from the research in this reporting period.

- Wavy fibers lower the interfacial stresses and thus increase the composite strength significantly.
- The wavy fiber composite studied has a lower stiffness.
- For the same fiber volume fraction, the composite with thinner fibers has a greater strength than the composite with thicker fibers.

I.6 References

I.1 Y.T. Zhu, J. A. Valdez, I. J. Beyerlein, S. Zhou, C. Liu, M. G. Stout, "Mechanical properties of bone-shaped short fiber reinforced composites," *Acta Materialia*, Vol. 47, 1999, pp. 1767-1781.

I.2 H. Jiang, J. A. Valdez, Y. T. Zhu, I. J. Beyerlein, T. C. Lowe, "The strength and toughness of cement reinforced with bone-shaped steel wires," *Composites Science and Technology*, Vol. 60, 2000, pp.1753-1761.

I.3 Q.-G. Zeng and C.T. Sun, "Novel Design of a Bonded Lap Joint," *AIAA Journal*, Vol. 39, No. 10, October 2001 pp. 1991-1996.

Part II: EFFECT OF FIBER SURFACE/VOLUME RATIO – FIBER PULL-OUT TEST

II.1 Introduction

Short fiber composites offer many advantages over continuous fiber composites mainly in that they are easy to manufacture complex shapes and that they often offer mechanical properties that are comparable to continuous fiber composites. The increasing use of nanomaterials as reinforcements in composites has recently received considerable attention due to potentially distinct property improvements. Among the various nanocomposites, nanoclay composites have been of increasing interest to many researchers [II.1]. The load transfer efficiency in short fiber composites is one of the most crucial factors affecting the overall composite properties. The load transfer efficiency depends on the nature of the reinforcement namely its shape, size and the surface area. One of the main differences between nanomaterials and conventional materials is that they have a very high surface area per unit volume. A nanomaterial can have substantially different properties from its bulk counterpart as many of these properties are governed by surface interactions.

In a composite, load in the matrix is transferred to the fiber. This load transfer has to take effect through the fiber/matrix interface. Thus, it is reasonable to expect good result if the fiber has a large surface area for a given volume. This is one of the reasons why nano materials are attractive as reinforcements for composites.

The effect of surface area on the stress load efficiency in short platelet type fiber composites is investigated. Fiber pull-out tests are conducted on a model composite with vinyl ester as the matrix and steel platelets of different thickness dimensions as reinforcements. Test results indicate that the thin fiber composite is more effective in load transfer than its thick fiber counterpart. A two-dimensional finite element with the application of appropriate boundary conditions was used for analysis of interfacial normal and shear stresses which provide the explain the test results.

The load transfer efficiency has been a subject of investigation for some time. Hsueh [II.2] developed a two-dimensional stress transfer model for platelet reinforcement. Hsueh et al. [II.3] analyzed the stress transfer in platelet-reinforced composites by performing analytical modeling and numerical simulations. Analysis by Tsai and Sun [II.4] indicated excellent load transfer efficiency in nanocomposites with uniformly

dispersed platelets on account of high aspect ratio of platelets. Recent studies by Sun et al. [II.5] on short platelet type fiber composites has demonstrated the potential to significantly improve the strength by increasing the surface area of the fiber. It was found that for the same fiber volume fraction thin fiber composites can have about 75% higher strength than the thick fiber composites. The success in achieving higher strengths by use of thinner platelet fibers has motivated the present study.

It is conceivable that for the same fiber volume in the composite, the thinner fibers provide more load transfer paths and thus lower interfacial stresses between the matrix and reinforcement. Since interfaces between the fiber and matrix are the weak links in the composite, the lowering of interfacial stresses is expected to result in higher composite strength. The objective of this research is to study the effect of surface area on the efficiency of load transfer in short fiber composites. Experiments on fiber pull-out are conducted using a model composite and the results are verified with the finite element analysis.

In this study, platelet type reinforcements are considered. For the ease of fabrication and conducting experiments, composite specimens having a vinyl ester matrix with steel platelets as reinforcements are manufactured with the platelet thickness in the range of 0.1-1mm. the width of the platelets is of the order of centimeters. Fiber pull-out tests are carried out to determine the load transfer efficiency.

II.2 Experiment

For easy fabrication and processing, a metal fiber composite system is chosen. The fiber platelet was made using the steel 1095 alloy. Steel sheets of 0.127mm (0.005in), 0.254mm (0.01in) and 0.508mm (0.02in) in thickness were cut into strips 4.6mm wide using a water jet cutting machine. The surface of the strip was then sanded by a sand paper (220 grit) to remove the top layer and was then cleaned thoroughly with acetone. In the next step, the steel platelet was cast into the matrix. Vinyl ester matrix was chosen which was made by thoroughly mixing vinyl ester resin with 1.75% (by weight) MEKP hardener. A mold was prepared with fiber in place and vinyl ester was poured around it. It was allowed to cure for 24 hrs at room temperature and then post cured at 250°F for 2 hrs. The final composite specimen has a fiber length of 18mm embedded inside the matrix. Once fully cured, the specimen was cut to the desired width. Fig. 1 shows the typical specimen geometry.

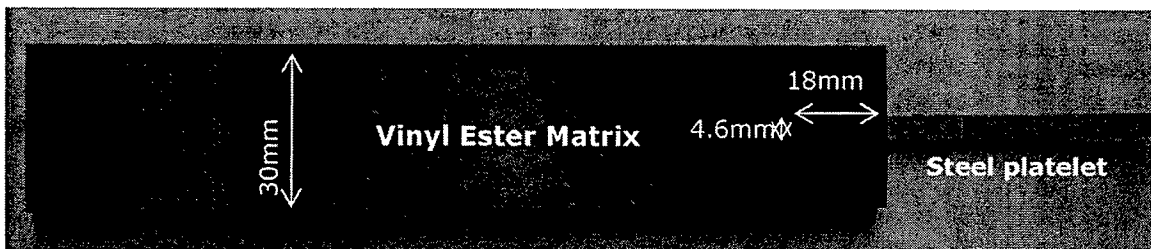


Figure I.1: Specimen details

Specimens were tested using a 22 kips MTS machine for tensile properties. The lower end of the specimen was gripped and the steel platelet was applied with a constant

displacement of 0.002mm/s. The stress-displacement curves for the specimens are shown in Fig. II.2. The pull-out stresses for each thickness are compared in Table II.1.

Table II.1 pull-out stresses for thin, thick, and thicker fiber specimens

Specimen #	Thin Fiber (MPa)	Thick Fiber (MPa)	Thicker Fiber (MPa)
1	834.51	708.62	576.45
2	834.76	692.16	559.21
Average	834.64	649.74	502.75

Failure/pullout modes for all of the specimens were similar. When loaded, the fiber platelets transfer the load to the surrounding matrix. As the load in the fiber platelet was increased further, the specimens experienced a sudden pullout which represents the point when no more load can be transferred to the matrix. Figure II.3 shows the de-bonded fiber and matrix after pullout. The sudden drop in the stress values in Figure II.2 represent the point of pull out. As can be seen from Figure II.2, the thick fiber specimens (0.02in) fractured at the point of pull out. To ascertain that this actually was the pullout point, we tested a couple of more specimens of the same width and a couple of specimens with a wider matrix. The tests for the subsequent set of specimens did reflect pull out at about the same stress value. If loaded beyond the pullout point, the fiber platelet experienced frictional sliding. The wavy nature of the stress-displacement curve for 0.005in fiber is due to relatively quicker load build up than its thicker counterparts.

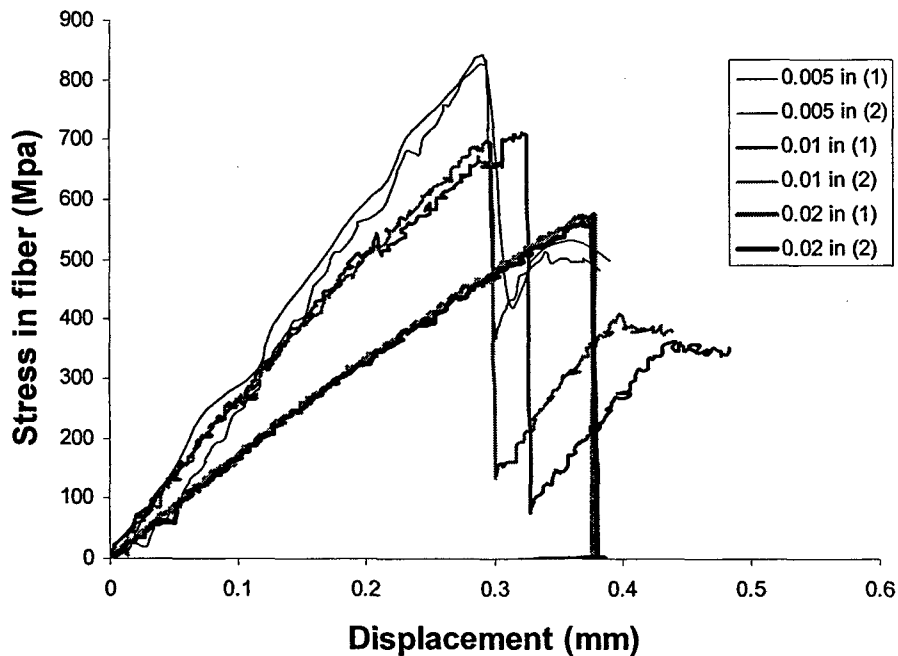


Figure II.2: Stress-displacement curve for fiber pull out tests

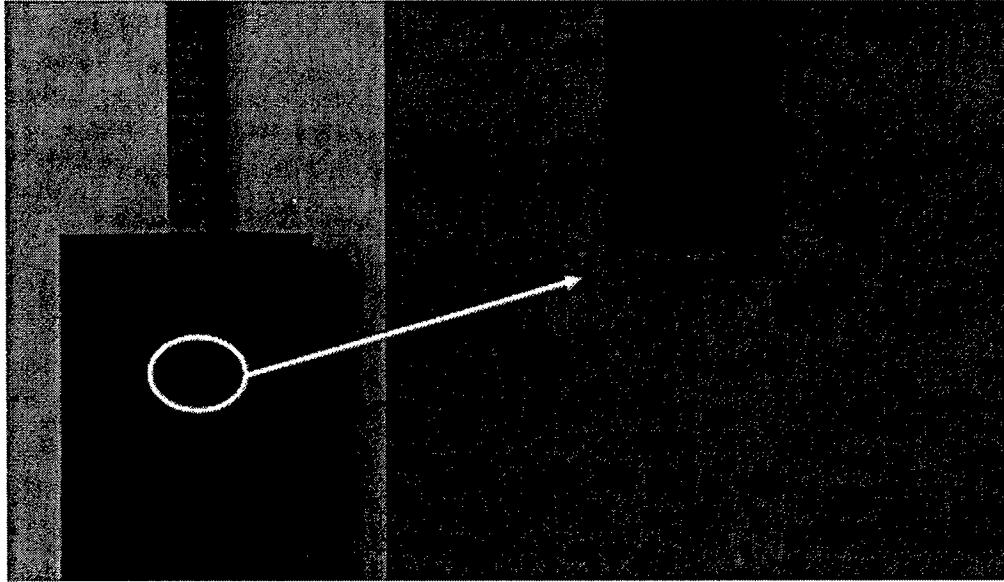


Figure II.3: Debonding of fiber and matrix after initial pullout

The test results presented in Figure II.4 indicate that thinner fibers yield a higher pullout stress than the thicker fibers. As the thickness of the fiber is reduced, the pullout stress increases. There is an increase of about 30% for each reduction in the thickness of the fiber. This increase can be attributed to the fact that by having same volume fraction of fibers and increasing the contact area between the matrix and fibers, there is a better and more efficient stress transfer from fiber to matrix and vice versa.

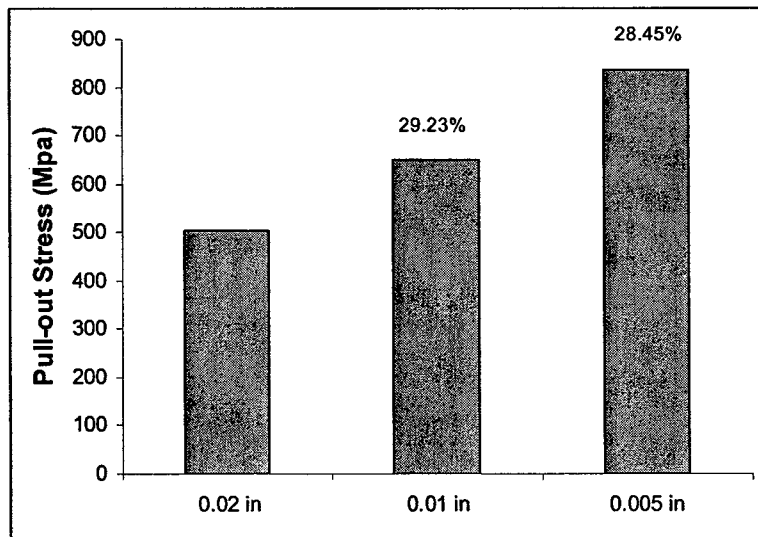


Figure II.4: Comparison of average pullout stress

II.3 Finite Element Analysis

To understand better the effect of thickness on the stress transfer efficiency of short fiber composites, finite element analyses were performed by modeling the thick (0.508mm or 0.02in) and thin fiber (0.254mm or 0.01in) composite specimens in the commercial finite element code ABAQUS. The stress distributions along the fiber and the interface were studied. A two-dimensional finite element model as shown in Fig. II.5 was constructed. Proper boundary conditions were applied and the fiber was pulled by a uniform stress of 1 MPa. The thickness of the epoxy was set as 6.5mm and the embedded length of the fiber was taken to be 18mm. Linear plane strain elements (Q4-4 noded linear quadrilateral) were used for the analysis. The area near the interface was finely meshed (Fig. II.6) so as to correctly capture the interfacial stress distribution. Identical element sizes were used in analyses in order to enable comparison of stresses. The elastic moduli and Poisson's ratios for the fiber and the matrix were taken to be 165GPa, 3.6GPa and 0.3, 0.36, respectively.

Of interest are the interfacial stresses in the composite model. Figs. II.7 and II.8 show the distributions of interfacial normal and shear stresses for the thick and thin fiber respectively. These stress components are referenced to the local tangential and normal directions of the fiber.

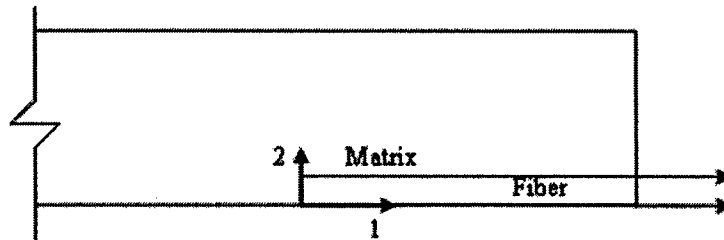


Figure II.5 Finite Element Model

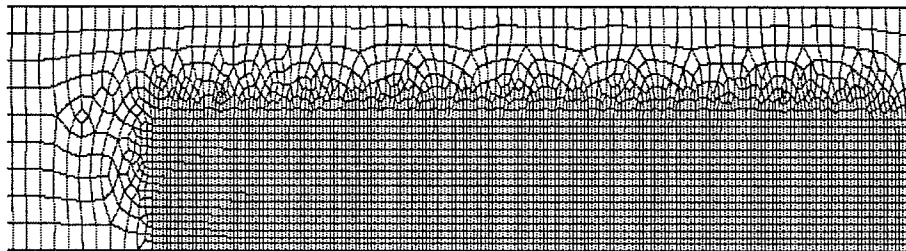


Figure II.6 Finite element mesh (not to scale)

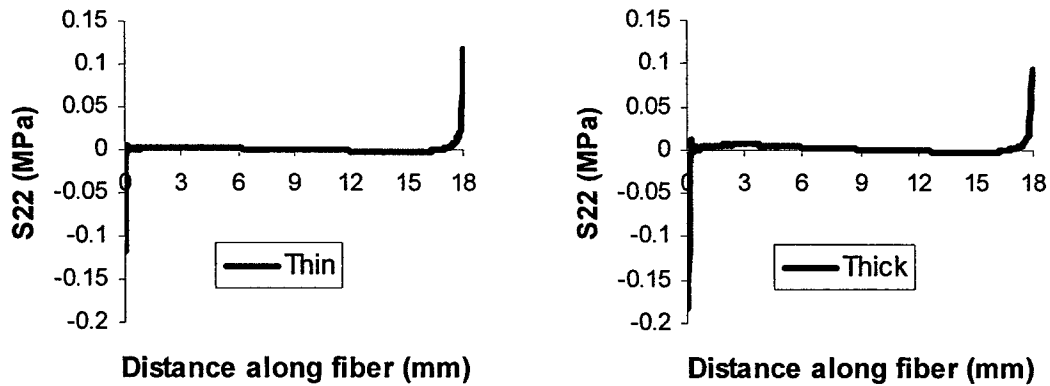


Figure II.7 Distribution of interfacial normal stress

From Figure II.7 we can see that both thin and thick fiber composites have a significant normal stress "singularity" at the embedded end and the location free end. Near the embedded end (0 mm) the thicker fiber has about 57% higher stress values than the thin fiber. Also there is a considerable difference in their shear stress distributions (Figure II.8). The shear stress concentration in the thin fiber composite is observed to be less severe than the thick fiber composite. These interfacial stresses near the embedded end for thicker fiber are about 30% more than those for the thin fiber. From the result of finite element analysis, it can be concluded that on account of lower interfacial normal stress and shear stress concentration, the thin fiber composites outperform the thick fiber composites.

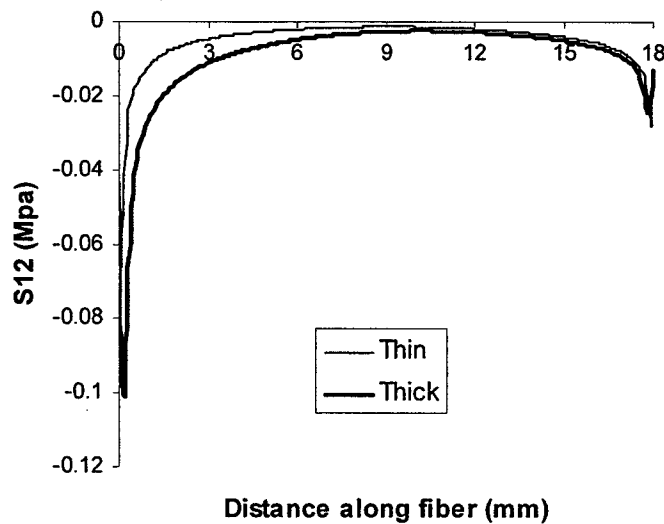


Figure II.8 Interfacial shear stresses

II.4 Conclusion

Increasing the surface area can significantly increase the load transfer efficiency of platelet type composites. For the same fiber volume fraction, the thin fiber composites exhibit higher pullout stresses than the thick fiber composite. On account of increased surface area of fiber platelet and hence the load transfer paths, there is a reduction in interfacial normal and shear stresses which results in higher composite strengths.

II.5 References

II.1 T.J. Pinnavaia, and G.W.Beall, *Polymer-Clay Nanocomposites*, John Wiley & Sons Ltd, New York, 2000.

II.2 Hsueh, C. (), "A Two-dimensional Stress Transfer Model for Platelet Reinforcement", *Composites Engineering*, 4(10), 1994, pp.1033-1043.

II.3 C.H. Hsueh, E.R. Fuller Jr., S.A. Langer, and W.C. Carter, "Analytical and Numerical Analyses for Two-Dimensional Stress Transfer", *Materials Science and Engineering A*, 268, 1999, pp.1-7.

II.4 Tsai J. and Sun C.T., "Effect of Platelet Dispersion on the Load Transfer Efficiency in Nanoclay Composites", *J Composite Materials*, Vol. 38, No 7, 2004, pp. 567-579.

II.5 C.T. Sun, A. Deo and H. Qian, "Effects of shape and surface area of fiber in short fiber composites, 45th AIAA SDM conference, 2004.

Part III: EFFECT OF REINFORCEMENT SIZE ON MODULUS AND STRENGTH

III.1 Introduction

In short fiber composites including nanocomposites, the load transfer efficiency among fibers is crucial in effecting superior composite properties. It is conceivable that this load transfer efficiency depends on the shape, aspect ratio, and surface area of the fiber. The effect of surface area of the reinforcing element is of particular importance because of the increasing use of nano particles in nanocomposites. It is well known that for the same volume, a material at nano scale possesses much greater surface areas than at larger scales. It is evident that more surface areas mean more load transfer paths and, thus, lower interfacial stresses between the reinforcement and the matrix. The lowering of interfacial stresses is expected to lead to higher composite strengths. In the previous sections, we used model composites to reach the following conclusions: 1) Wavy fibers lower the interfacial stresses and thus increase the composite strength significantly; 2) for the same fiber volume fraction, the composite with thinner fibers has higher strength than the composite with thicker fibers, 3) result of fiber (platelet) pull-out tests indicates that thinner fibers gave a higher pull out strength than thicker fibers. The increase was about 30% for each 50% reduction in the thickness of the fiber.

The effect of particle size on mechanical performance of composites has been addressed by many authors. Leidner and Woodhams [III.1] demonstrated that the tensile strength of glass beads/polyester composites increases as the size of glass beads decreases. Gent [III.2] used an analytical study based on Griffith's fracture criterion to conclude that the stress inducing debonding of particle from matrix increases with decreasing particle size. Needleman [III.3] reached a similar conclusion based on a numerical study using a cohesive zone model. Gent and Park [III.4] conducted experimental observations with a single glass bead embedded in elastomer specimens and found that the stress level associated with matrix cavitation and particle/matrix debonding becomes higher as the inclusion size becomes smaller. In recent years, various nanomaterials with various unique properties have been produced. Due to their much greater reactive surface area per unit volume compared that of larger particles, nanomaterials together with polymers have been explored to form nanocomposites. Consequently, the interest in the subject of particle size effect at the nano meter scale has been revived.

Ng et al. [III.5] measured tensile properties and scratch resistance of TiO_2 (32 nm)/epoxy nanocomposites and compared them to those of composites with micron size TiO_2 (0.24 μm). In comparison, higher failure strain and scratch resistance were observed in the nanocomposite [III.5]. Flexural modulus and strength measurements were performed with alumina (Al_2O_3) particles of 40 nm, 1 μm and 3 μm in diameter with a vinyl ester resin [III.6]. The flexural modulus was not affected by the particle size, but the strength was found to be lowered as the particle size decreased. The decrease in strength relative to the particle size was attributed to poor dispersions of nanoparticles in the composite.

In order to understand the size effect of all scales in particulate composites, the failure mechanism and mechanical properties in these composites must be understood. In this study, systematic experimental programs together with finite element analyses were performed on polymeric composites reinforced with spherical particles. The particle sizes considered ranged from macro (0.5 mm) to nano (15 nm) scale. Mechanical properties of the composites were measured through tensile tests. With the aid of a specially designed load frame, microscopic failure process in the composite was observed during tension tests. The effect of nanoparticle dispersion on composite failure was studied with SEM (Scanning Electron Microscope) and TEM (Transmission Electron Microscope) images.

The experimental observations were analyzed numerically. For the composites with microparticles, finite element analyses were performed to investigate the particle size effect on their failure mechanism. For the composites with nanoparticles, molecular dynamics simulations were carried out. In this paper, the authors present the results of the finite element analyses. The analysis results by molecular simulations will be included in our next paper.

Finite element analyses of the debonding interfacial crack were performed taking into account particle size as well as partial debonding between particle and matrix. The effect of particle and interfacial crack size on the total strain energy release rate was investigated with the modified crack closure method [III.7]. The mode mixity was calculated based on the displacement ratio method [III.8, III.9]. Interfacial fracture toughness of single glass bead/vinyl ester matrix composites was evaluated by computer aided image analysis associated with the applied loading history. The effect of particle size and mode mixity of the interfacial crack on the fracture toughness was investigated.

III.2 Experimental Investigation

The effect of particle size on Young's modulus and failure stress by tensile loading are presented in Figures III.1 and III.2, respectively. Both properties are normalized with the neat resin properties. From Figs. III.1a and III.1b, it is evident that, the composite Young's modulus is influenced by particle volume fraction and modulus rather than its size if the particle size is of micro scale. However, as the size of alumina particles reduces to 50 nm and 15 nm in diameter, the composite Young's modulus increases as shown in Figure III.1b.

As seen in Figures III.2a and III.2b, the strength of the composite is significantly dependent on the size of particles. The tensile strength increases as the particle size decreases except for the composite with alumina nanoparticles of 3% volume fraction. We attribute this strength weakening to the result of poor dispersion of the nanoparticles in the 3% nanocomposite.

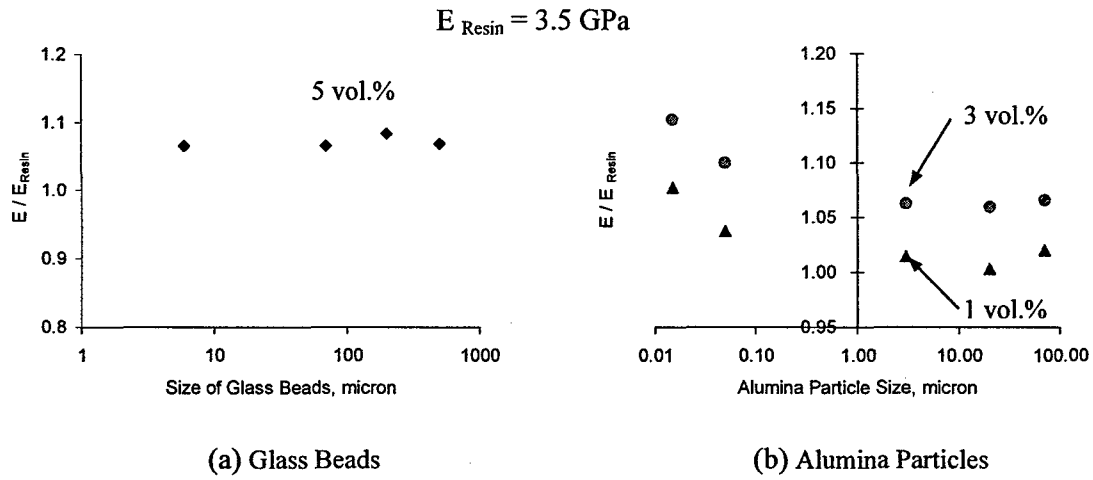


Figure III.1 Effect of particle size on Young's modulus of composites

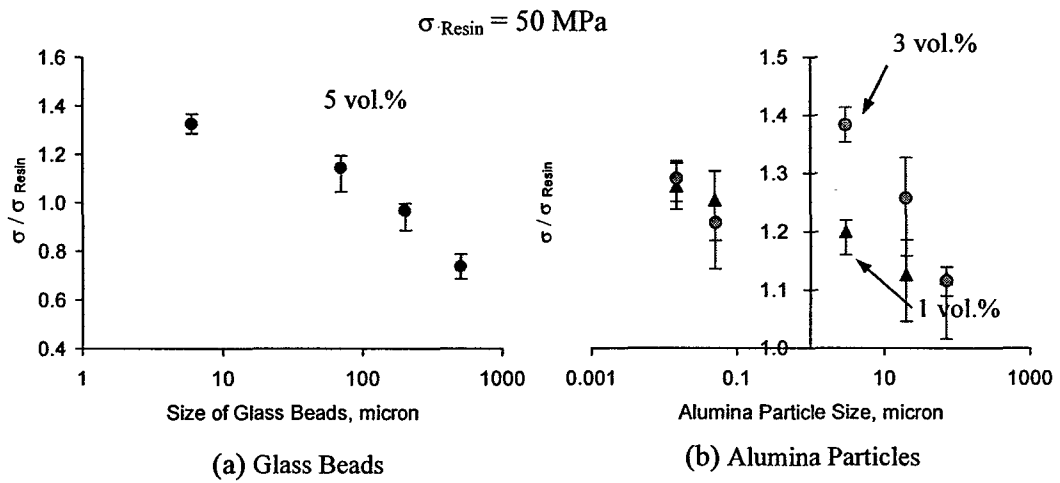
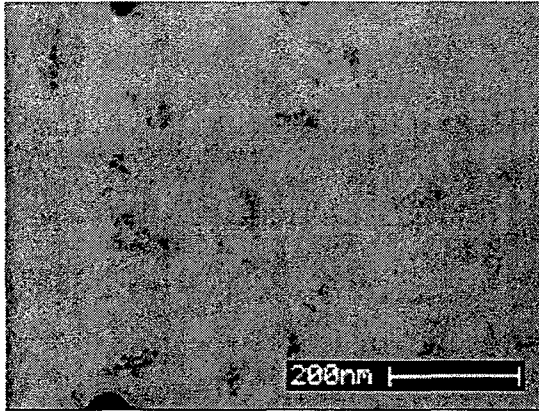
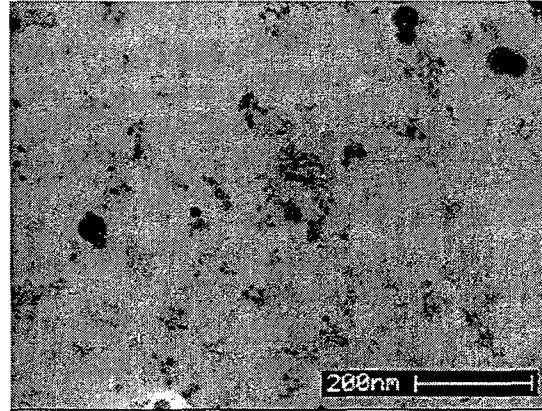


Figure III.2 Effect of particle size on tensile strength of composites

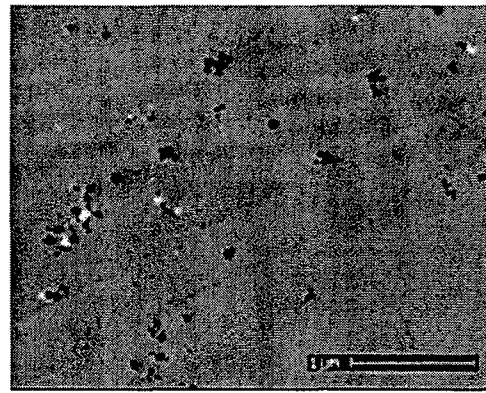
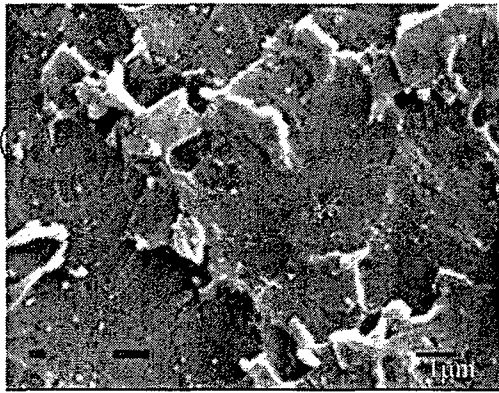


(a) 1 vol. % Alumina Particles

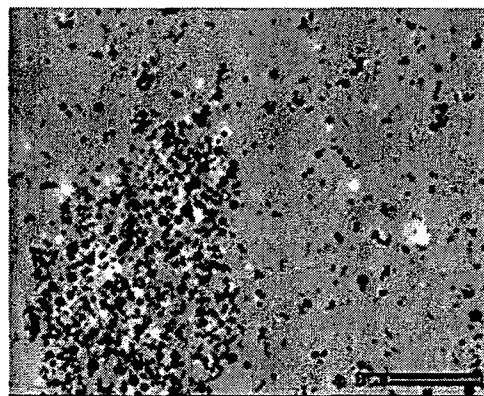
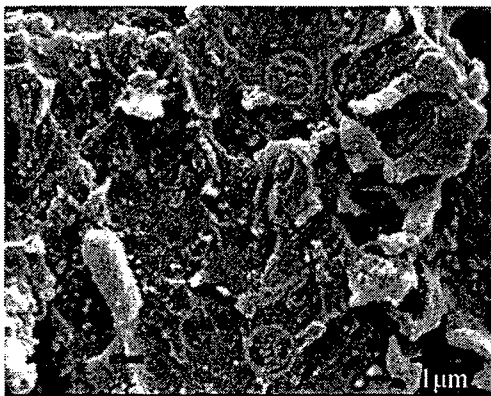


(b) 3 vol. % Alumina Particles

Figure III.3 TEM images of nanocomposites with 15 nm alumina particles



(a) SEM (Left) and TEM (Right) images of nanocomposite with 1 vol. % alumina particles (Circles indicate particle clusters in SEM image.)



(b) SEM (Left) and TEM (Right) images of nanocomposite with 3 vol. % alumina particles (Circles indicate particle clusters in SEM image.)

Figure III.4 SEM and TEM images of nanocomposites with 50 nm alumina particles

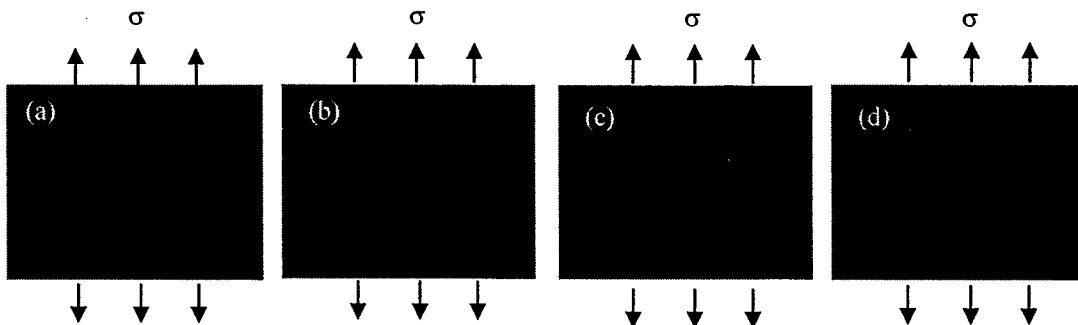


Figure III.5 Demonstration of failure progression; (a) debonding Initiation at one pole of the particle, (b) debonding growth at the pole, (c) debonding appearance at the opposite-pole, (d) full extent of debonding

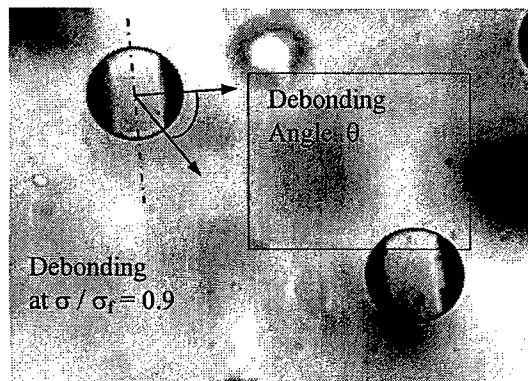


Figure III.6 Partially debonded particles and definition of debonding angle

All composites experienced failure initiation in the form of debonding between matrix and particles. The debonding initiation appeared mostly at one pole of the particle in the direction of the applied tension. The number of debonded particles and the debonded area grew as the applied stress increased. For particles smaller than 70 μm in diameter, debonding area at one pole grew to a certain size, and then stopped. Subsequently, debonding appeared on the opposite pole of the particles. Eventually, debonding growth ceased at the applied stress of about 80-90% failure stress. At that stage, the debonding angle measured from the pole to the front of the debonded region was around 52-62 degrees. The images in Figure III.5 show the sequence of the failure progression. Figure III.6 shows an image of debonded particles and measured debonding angle at the applied stress of 90% failure strength.

III.3 Finite Element Analysis

Particle/matrix debonding was treated as an interfacial fracture problem. The effect of particle size on debonding growth was investigated in terms of total strain energy release rate, fracture mode mixity and interfacial fracture toughness. Analysis results were compared with experimental observation of the debonding growth behavior.

The cylindrical cell is axisymmetric with respect to the loading axis and is employed as the RVE of the composite. For the RVE with debonding, two models were constructed in consideration of one-pole and symmetric (two-pole) debondings. The RVE with the one-pole debonding was modeled with a full axisymmetric plane. For the symmetric debonding, a half axisymmetric plane was taken for the finite element model.

The total strain energy release rate has been used as a fracture parameter for interfacial crack propagation. In this study, the modified crack closure technique was employed to evaluate the total strain energy release rate. In the technique, the strain energy released during crack extension is obtained by calculating the work needed to close the opened crack surfaces. The total strain energy release rates of particle/matrix debonding for different particle sizes corresponding to a tensile load of 1 MPa are presented in Figure III.7. The particle sizes considered were 1 μm , 5 μm , and 10 μm in diameter. Interfacial crack propagation was simulated by increasing the debonding angle from 20 degree to 80 degree. It is clearly seen in Figure III.7 that G_T of the interfacial crack decreases as the particle size decreases. This implies that, for the same interfacial toughness, it would require a greater driving force G_T to grow debonding at a smaller particle. As a result, smaller particles could enable the composite to carry higher loads.

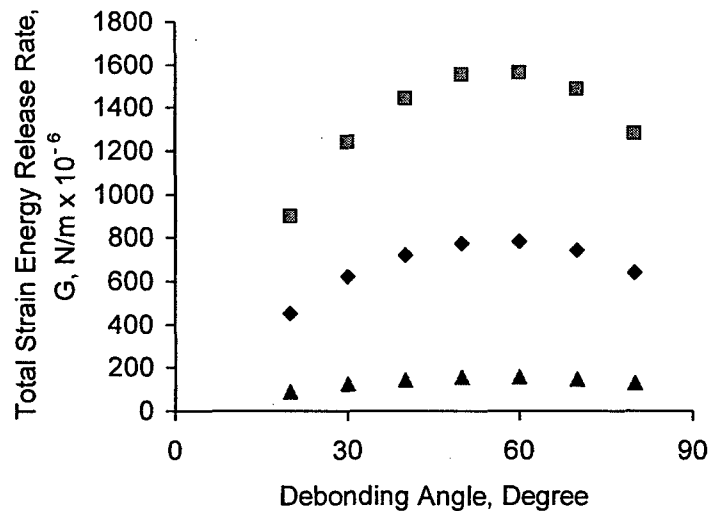


Figure III.7 Effect of Particle Size on Total Strain Energy Release Rate of One Pole Debonding (Triangles, diamonds and squares indicate the particle size of 1 μm , 5 μm and 10 μm in diameter, respectively; Applied load is 1MPa.)

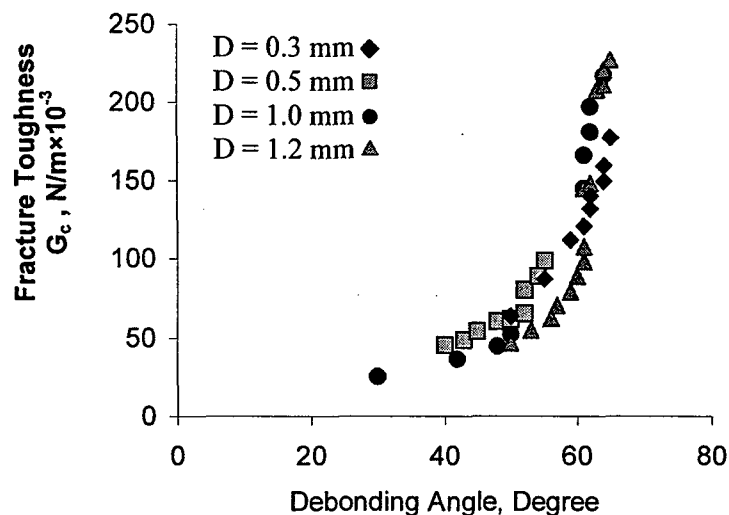


Figure III.8 Fracture toughness with respect to debonding angles (symbols of diamond, square, circle and triangle represents particle size of 0.3 mm, 0.5 mm, 1.0 mm and 1.2 mm in diameter.)

Fracture toughness measurement of the spherical inclusion/matrix interfacial crack was performed with specimens of a single glass bead embedded in the vinyl ester matrix. In order to take into accounts the effect of the particle size on toughness, different size glass beads were used in the measurement. Interfacial fracture toughness was measured with glass beads of 0.3 mm, 0.5 mm, 1.0 mm and 1.2 mm in diameter. Fracture toughness of those interface cracks was obtained from the total strain energy release rates resulting with the measured debonding stresses. The result is presented in Figure III.8 in terms of the critical energy release rate vs. debonding angle. From the result, it is reasonable to state that there is no significant effect of the particle size on fracture toughness at least for mm size particles. In addition, the fracture toughness is seen to increase exponentially when the sliding fracture mode becomes dominant. It may explain the fact that debonding cracks cease to grow beyond debonding angles of 52-62 degrees.

III.4 Molecular Dynamics Simulation

Models of nanocomposites consisting of amorphous linear polymer chains and rigid nanoparticles of various sizes were selected for molecular dynamics simulations. In this study, the polymer chain was a bead-spring chain with 100 monomers. Nanoparticles were generated with the same beads of the polymer beads. However, since nanoparticles are generally heavier than polymers, the mass of the beads used to generate the nanoparticles were set to be double to that of the polymer beads. The nanoparticles were

constructed in a simple cubic crystal structure. In addition, they were maintained rigid during simulations with constraint of the distance between the centers of the beads.

All non-bonded beads interacted according to the Lennard-Jones pair potential,

$$U_{LJ}(r) = 4u_{pk} \left[\left(\frac{l_r}{r_{ij}} \right)^{12} - \left(\frac{l_r}{r_{ij}} \right)^6 \right], \quad \text{where } k = n, p \quad (1)$$

where l_r is the equilibrium distance of bead pairs and the basic length unit of the Lennard-Jones potential; r_{ij} is the separation between beads i and j ; the subscripts n and p represent nanoparticle and polymer, respectively. Thus, the energy unit u_{pp} and u_{pn} indicate the strength of polymer-polymer and polymer-nanoparticle interactions, respectively. For computational convenience, the strength of polymer-polymer interactions u_{pp} was set to be unity, *i.e.*, $u_{pp} = 1$. The potential was truncated to yield zero energy and force at the cut-off radius $r_c = 2.2l_r$.

Adjacent bonded beads in a chain interacted with the FENE potential,

$$U_{FENE}(r) = -0.5kR_o^2 \ln \left[1 - \left(\frac{r_{ij}}{R_o} \right)^2 \right] + 4u_{pp} \left[\left(\frac{l_r}{r_{ij}} \right)^{12} - \left(\frac{l_r}{r_{ij}} \right)^6 + \frac{1}{4} \right], \quad (2)$$

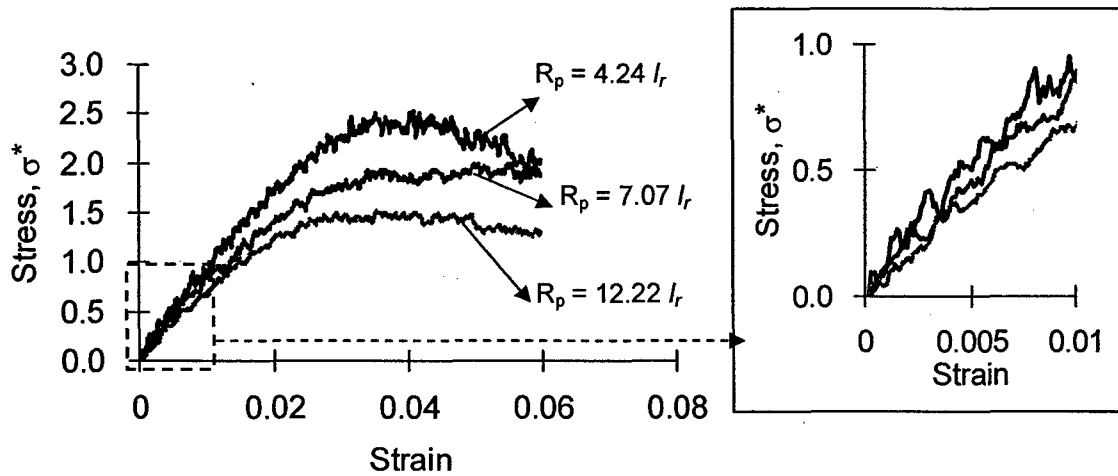
where $R_o = 1.5 l_r$ and $k = 30 u_{pp}/l_r^2$. In Equation (2), the first term generates attractive force, and the second Lennard-Jones term does repulsive force. The first term allows the bond to extend to R_o , which is the maximum extent of the bond. If the bond length exceeds R_o , the first term is conditioned to generate infinite attractive force, so that it can be avoided to have broken bonds during simulations. The second term is cut off at $r_c = \sqrt[6]{2}l_r$, where the minimum of the Lennard-Jones potential takes place.

Three different strengths of polymer-nanoparticle interactions were considered using the Lennard-Jones potential. By comparing to the interaction strength u_{pp} of the polymer chains, these polymer-nanoparticle interactions were named as strong, neutral, and weak interactions, respectively. For the strong interaction, we set $u_{pn} = 2u_{pp}$, for the neutral interaction, $u_{pn} = u_{pp}$, and for the weak interaction, $u_{pn} = 0.5u_{pp}$.

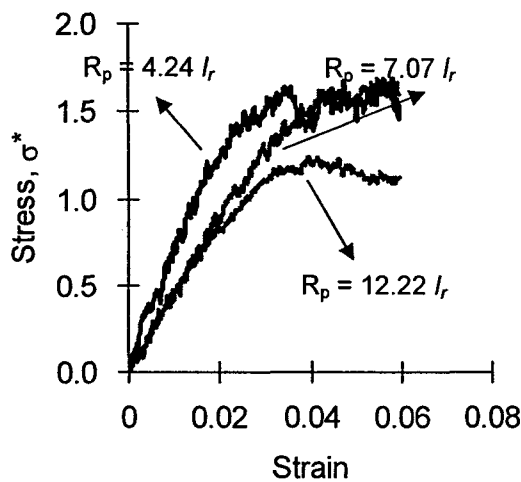
Simulations of simple tension tests on the nanocomposites constructed as described above were performed by applying uniform uniaxial extension on the simulation box. This was done by allowing the volume and shape of the simulation box to change. On the lateral surfaces of the simulation box, stress free conditions were imposed. All simulations were performed using a molecular dynamics simulation package LAMMPS that was developed at Sandia National Laboratories.

In Figure III.9, stress-strain curves of nanocomposites with 18% volume fraction of nanoparticles for different polymer-nanoparticle interactions, volume fractions, and nanoparticle sizes are presented. The Young's moduli are summarized in Figure III.10. It is evident from Figures III.9 and III.10 that both the modulus and load-carrying capacity of the nanocomposite with the strong or neutral polymer-nanoparticle interaction increase as the size of the nanoparticle decreases. For the weak interaction, there is little

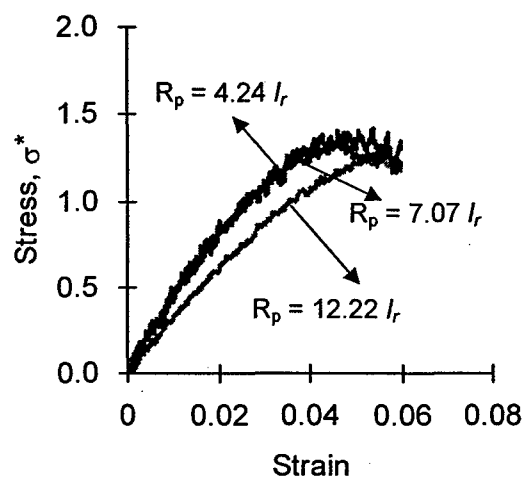
improvement resulting from a size decrease in the nanoparticle from $7.07l_r$ to $4.24l_r$, as seen in Figure III.9c.



(a) Strong polymer-nanoparticle interactions



(b) Neutral Interactions



(c) Weak Interactions

Figure III.9 Effect of nanoparticle size on tensile behavior of nanocomposites (volume fraction = 18% and $\sigma^* = \sigma(l_r^3)/u_0$)

The increase of modulus in nanocomposites with smaller nanoparticles may be viewed from the stress distribution near the nanoparticle. A volume-averaged stress was used to indicate the local stress level in the polymer near the nanoparticle. Figures III.11-III.13 present the distributions of the averaged stress component in the loading direction along the distance normalized by the nanoparticle radius. The applied strain is 1% engineering strain and the volume fraction 18%.

It is shown in Figures III.11 - III.13 that the stronger polymer-nanoparticle interaction induces higher stresses near the nanoparticle, and that smaller nanoparticles cause higher

stresses around the nanoparticle. As shown in Figure III.13, the stress distributions in the composites with three different sizes of nanoparticles, respectively, show little difference if the polymer-nanoparticle interaction is weak. This explains why, in the case of weak particle/polymer interactions, there is no appreciable nanoparticle size effect on Young's modulus of the nanocomposite.

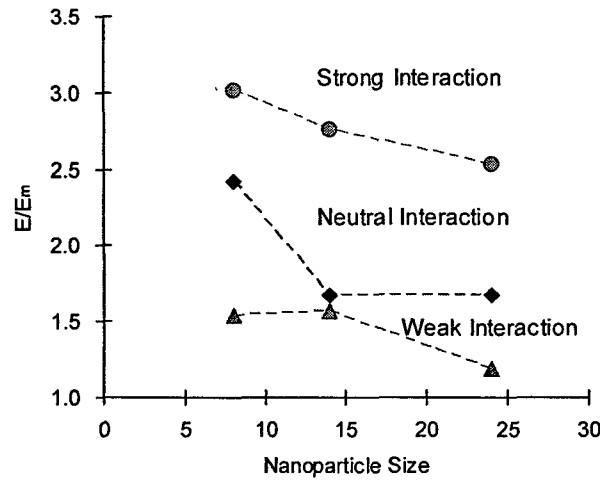


Figure III.10 Effect of nanoparticle size and polymer-nanoparticle interaction strength on Young's modulus of nanocomposites ($E_m = 27.3$; Young's modulus of the polymer matrix; volume fraction = 18 %.)

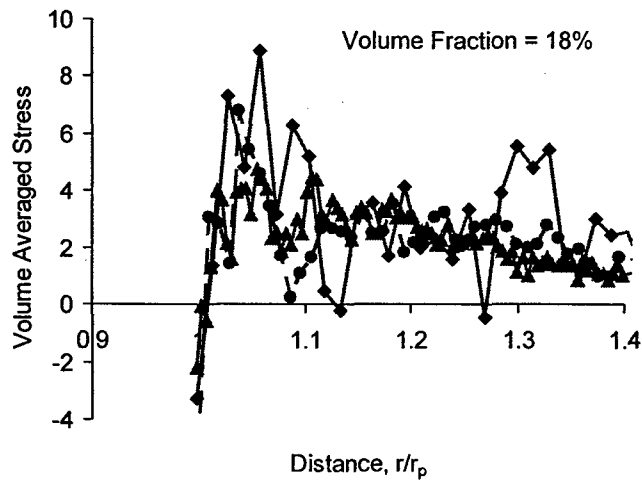


Figure III.11 Volume averaged stress distributions around the nanoparticles with the strong polymer-nanoparticle interactions (diamonds, circles and triangles indicate the nanoparticle radii of $4.24l_r$, $7.07l_r$ and $12.22l_r$, respectively.)

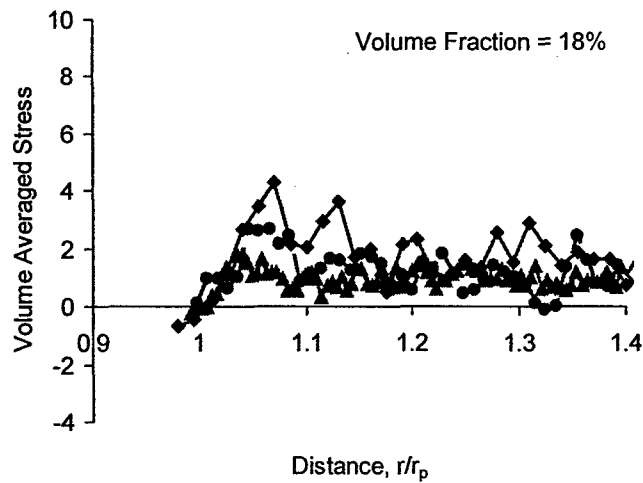


Figure III.12 Volume averaged stress distributions around the nanoparticles with the neutral polymer-nanoparticle interactions (diamonds, circles and triangles indicate the nanoparticle radii of $4.24l_r$, $7.07l_r$, and $12.22l_r$, respectively.)

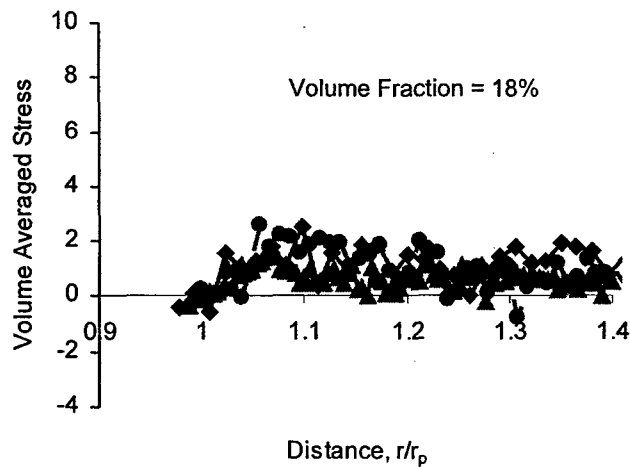


Figure III.13 Volume averaged stress distributions around the nanoparticles with the weak polymer-nanoparticle interactions (diamonds, circles and triangles indicate the nanoparticle radii of $4.24l_r$, $7.07l_r$, and $12.22l_r$, respectively.)

III.5 Conclusion

A systematic experimental and numerical study has been conducted to determine the effect of particle size on elastic modulus, tensile strength, and particle/matrix debonding fracture behavior of particulate composites. The major findings are summarized as follows.

- 1) The Young's modulus of a particulate composite is not influenced by the size of the particle if it is of micron or larger sizes. However, the composite Young's modulus is enhanced with decreasing particle sizes at nano scale. It is considered from molecular dynamics simulations that this enhancement of modulus by nanoparticles may be attributed to a stiff polymer layer formed by highly dense polymer beads around nanoparticles. Through the stiff polymer region, higher stresses are transferred near the nanoparticles with smaller particles and stronger polymer-nanoparticle interactions. Moreover, it was observed that in order to increase Young's modulus with decrease of nanoparticle size, the interaction strength between polymer chains and nanoparticles needs to be larger than that between polymer chains themselves.
- 2) The tensile strength of particulate composites can be improved with decreasing particle size. However, due to the likely poor dispersion of nanoparticles at higher particle loading, composites with 3 vol.% nanoparticles resulted in a lower tensile strength than that with microparticles.
- 3) From the experimental observation together with a numerical analysis, it was found that the effect of particle size on particle/matrix interfacial fracture toughness is negligible. However, the interfacial crack for smaller particles requires higher applied stress to grow because the energy release rate decreases as the particle size decreases for the same applied stress. It was also observed that the fracture toughness increases exponentially when the sliding mode of the interfacial crack prevails.

III.6 References

- III.1 Leidner, J. and R. T. Woodhams, "The Strength of Polymeric Composites Containing Spherical Fillers," *Journal of Applied Polymer Science*, Vol. 18, 1974, pp. 1639-1654.
- III.2 Gent, A. N., "Detachment of an Elastic Matrix from a Rigid Spherical Inclusion", *Journal of Materials Science*, Vol. 15, 1980, pp. 2884-2888.
- III.3 Needleman, A., "A Continuum Model for Void Nucleation by Inclusion Debonding", *Journal of Applied Mechanics*, Vol. 54, 1987, pp. 545-531.
- III.4 Gent, A. N. and B. Park, "Failure Processes in Elastomers at or near a Rigid Spherical Inclusion," *Journal of Materials Science*, Vo. 19, 1984, pp. 1947-1956.
- III.5 Ng, C. B., L. S. Schadler and R.W. Siegel, "Synthesis and Mechanical Properties of TiO₂-Epoxy Nanocomposites", *NanoStructured Materials*, Vol. 12, 1999, pp. 507-510.

III.6 Lopez, L., B. M. K. Song and H.T. Hahn, "The Effect of Particle Size in Alumina Nanocomposites", presented at the ICCM 14th Conference, San Diego, CA, July 14-18, Paper # 1743, 2003.

III.7 Rybicki, E. F. and M. F. Kanninen, "A Finite Element Calculation of Stress Intensity Factors by a Modified Crack Closure Integral", *Engineering Fracture Mechanics*, Vol. 9, 1977, pp. 931-938.

III.8 Sun, C. T. and W. Qian, "The Use of Finite Extension Strain Energy Release Rates in Fracture of Interfacial Cracks", *International Journal of Solids and Structure*, Vol. 34, 1997, pp. 2595-2609.

III.9 Ikeda, T. and C. T. Sun, "Stress Intensity Factor Analysis for an Interface Crack between Dissimilar Isotropic Materials under Thermal Stress", *International Journal of Fracture*, Vol. 111, 2001, pp. 229-249.

Part IV: PUBLICATIONS

- U.V.R.S. Turaga and C.T. Sun, "An Investigation of Adhesive Single-lap Joints with Attachments," *44rd AIAA/ASME/ASCE/AHS/ASC Structures, Structural Dynamics, and Materials Conference*, Norfolk, Va, April 7 - 10, 2003.
- C.T. Sun and U.V.R.S. Turaga, "An Improved Method for Joining Composites," *Proceedings of the 14th International Conference on Composite Materials (ICCM-14)*, San Diego, July 14 - 18, 2003.
- H. Qian and C.T. Sun, "Performance of a Composite Double Strap Joint with Attachments," *Joining and Repair of Composite Structures*, (Keith T. Kedward and Hyonny Kim, Editors) *ASTM STP 1455*, American Society of Testing and Materials, West Conshohocken, PA, 2004, pp. 55-66.
- J. Cho, M.S. Joshi, and C.T. Sun, "Effect of Inclusion Size on Mechanical Properties of Polymeric Composites with Micro and Nano Particles," to appear in *Composites Science & Technology*.
- C.T. Sun, A. Deo, and H. Qian, "Effects of Shape and Surface Area of Fiber in Short Fiber Composites," *45th AIAA/ASME/ASCE/AHS/ASC Structures, Structural Dynamics, and Material Conference*, Palm Springs, California, April 19-22, 2004.
- A. Deo and C.T. Sun, "Effect of Thickness of Platelet on Load Transfer Efficiency in Platelet-Reinforced Composites," *19th Technical Conference, American Society for Composites*, Atlanta, Georgia, October 17-19, 2004.
- J. Cho and C.T. Sun, "Failure Mechanisms in Polymer Composites Containing Micro- and Nano- Particles," *19th Technical Conference, American Society for Composites*, Atlanta, Georgia, October 17-19, 2004.

- J. Cho and C.T. Sun, "A Molecular Dynamics Simulation Study of Particle Size Effect on Mechanical Properties of Polymeric Nanocomposites," ASME International Mechanical Engineering Congress & Exposition, Orlando, Florida, November 6-11, 2005.